Tikrit Journal of Engineering Sciences (2024); 31(3): 177-191
DOI: http://doi.org/10.25130/tjes.31.3.17

IRAQI Academic Scientific Journals

ISSN: 1813-162X (Print); 2312-7589 (Online)
Tikrit Journal of Engineering Sciences
available online at: http://www.tj-es.com

TJES Tikrit Journal of Engineering Sciences

Assessment of Perforated Double-Pass Solar Air Heater Using Parametric Interaction Analysis for Performance Enhancement in Solar Thermal Systems

*Ali A. Gitan, Abdulbari H. Mohammed **

Mechanical Engineering Department, College of Engineering, Tikrit University, Tikrit, Iraq.

Keywords:

Correlation; Design of experiment; Double pass; Interaction of factors; Perforated absorber; Solar air heater.

Highlights:

- *Perforation improves double-pass solar air heater performance due to the mixing effect.*
- *Performance assessment by a parametric study is based on the interaction of factors.*
- *Tests were conducted based on the design of the experiment approach to obtain correlations.*
- *Interaction percentage was 193 % for efficiency, while enhancement was 12.36%.*
- *A low perforation ratio and a high Reynolds number are the optimum parameters.*

ARTICLE INFO

Article history:

Received	30 June	2023
Received in revised form	06 Oct.	2023
Accepted	07 Nov.	2023
Final Proofreading	18 Aug.	2024
Available online	19 Aug.	2024

Citation: Gitan AA, Mohammed AH. **Assessment of Perforated Double-Pass Solar Air Heater Using Parametric Interaction Analysis for Performance Enhancement in Solar Thermal Systems**. *Tikrit Journal of Engineering Sciences* 2024; **31**(3): 177-191. http://doi.org/10.25130/tjes.31.3.17

*Corresponding author:

Abdulbari H. Mohammed

Mechanical Engineering Department, College of Engineering, Tikrit University, Tikrit, Iraq.

Abstract: The low performance of solar air heaters (SAHs) has been considered a drawback in commercializing solar thermal systems. The SAH performance is influenced directly by changing the level of the influential parameters. This work experimentally determines the optimum parameters for enhancing a perforated double-pass SAH performance. The interaction of factors related to the performance of circular staggered perforated double pass SAH was discussed based on the design of experiments (DOE) approach. Reynolds number values from 10000 to 30000 and perforation ratios from 3 to 7 were considered model design parameters, while temperature difference, useful heat gain, and thermal efficiency were adopted as responses for the correlating model. Three correlations corresponding to each response with two forms each (actual and coded) were obtained from the DOE analysis. The results revealed that the interaction percentage was 193% for efficiency and 148% for useful heat gain; however, it did not exceed 18% for the temperature difference. The optimum parameters obtained were 30000 for the Reynolds number and 3 for the perforation ratio. At high Reynolds numbers, the thermal efficiency enhancement of perforated SAH was 12.36% higher than the unperforated. The Reynolds number impact on thermal efficiency changed significantly as the perforation ratio varied.

تقييم سخان هواء شمسي مثقب ذي الممر المزدوج باستخدام تحليل تداخل العوامل المؤثرة لغرض تحسين الأداء في الأنظمة الشمسية الحرارية

علي احمد كَيطان، عبدالباري البياتي
قسم الهندسة الميكانيكية/ كلية الهندسة / جامعة تكريت / تكريت – العراق.

الخلاصة

تعتبر مشكلة الكفاءة القليلة لسخانات الهواء الشمسية عائقاً في تسويق الأنظمة الحرارية الشمسية. يتأثر أداء سخانات الهواء الشمسية بشكل مباشر بتغيير مستوى العوامل المؤثرة. يهدف هذا العمل الى تحديد العوامل المثلى عملياً من أجل تحسين أداء سخان هواء شمسي مثقب ذي الجريان المزدوج. تمت مناقشة تداخل العوامل المتعلقة بأداء سخان هواء شمسي مزدوج الجريان ذي صفيحة امتصاص مثقبة بثقوب دائرية ذات توزيع متداخل بناءً على طريقة تصميم التجارب. تمت دراسة عدد رينولدز بقيمة ١٠٠٠٠ الى ٣٠٠٠٠ ونسبة التثقيب بقيمة ٣ إلى ٧ كعوامل تصميمية للنموذج بينما تم اعتماد فرق درجة الحرارة، وكمية الحرارة المكتسبة، والكفاءة الحرارية كاستجابات لنموذج الارتباط. تم الحصول على ثلاثة ارتباطات مقابلة لكل استجابة مع شكلين لكل منهما (الفعلي والمشفّر) من خلال تحليل طريقة تصميم التجارب هذه. بينت النتائج أن نسبة التداخل كانت ١٩٣٪ للكفاءة الحرارية و١٤٨٪ لكمية الحرارة المكتسبة، بينما لم تتعد ١٨٪ لفرق درجات الحرارة. عند المستوى الأعلى لعدد رينولدز، تم تسجيل زيادة بنسبة ١٢,٣٦٪ في الكفاءة الحرارية بسبب التثقيب على عكس سخان الهواء الشمسي غير المثقوب. يغير عدد رينولدز تأثيره على الكفاءة الحرارية بشكل كبير عندما يتغير مستوى التثقيب.

الكلمات الدالة: ارتباط، تصميم التجارب، الممر المزدوج، تداخل العوامل، لوح امتصاص مثقب، سخان هواء شمسي.

1.INTRODUCTION

The global energy problem and the environmental effects of greenhouse gases due to fossil fuel burning call for renewable energy generation technology and energy demand reduction initiatives [1]. Solar energy is the most common available source among many energy sources and has the greatest potential to meet energy requirements without negative effects on the environment [2]. Solar air heaters (SAHs) are solar collectors utilizing solar energy in numerous applications, such as room heating, water desalinization, and drying agricultural products [3, 4]. SAHs are simple in construction, consisting of a thermally insulated duct, transparent cover, air blower, and absorber plate [5]. Diverse parametric studies have been conducted in different ways to consider the geometrical and/or operational factors of SAHs. Most of these works adopted the individual factor consideration to discuss the direct parametric effect on the SAHs' performance [6-11]. Generally, this method does not go through the statistical analysis of the experimental/numerical data. In contrast, the regression approach to analyze the collected data for SAHs has been followed by other works [12-14]. The results showed a good agreement between the predicted and measured performance. However, all these parametric studies adopted the direct (or main) effect of factors, while the considered parameters have another story. The interaction of factors can reveal more indirect impact generated when the behavior of one factor is influenced by changing the level of other factors. Dezan et al. [15] classified the interaction of factors into weak, moderate, and strong interactions when parametric and optimization analyses were studied for SAH with a vortex generator. Delta winglet pairs have been used to generate the vortex in the flow with a Reynolds number ranging from 5000 to 10000. Nine input parameters related to the configuration and distribution of the winglet pairs have been adopted. Higher performance enhancement was observed when the Reynolds number increased. In summary, determining the interaction effect on the response needs more analysis in the context of SAH performance enhancement. Researchers have presented many attempts and studies to improve the SAHs' performance by suggesting a double pass technique for different configurations of absorber plates. In this context, this SAH's performance improved by increasing the number of transverse fins between mesh layers [16]. The maximum efficiency of 75%, 82%, and 85.9% were found for 2, 3, and 6 fins, respectively. A significant enhancement in performance was recorded for double-pass SAH with a wire-mesh absorber [17]. The results showed a maximum efficiency of 62.50% was obtained when using the 7.5-cm high collector for the double-pass SAH and 55% for the single-pass SAH. Another double-pass SAH was modified using an artificial roughness with different configurations to increase its thermal performance [18-21]. In a different work, the double pass SAH efficiency increased by fixing aluminum cans on the absorber [22]. The mass flow rates were 0.03 kg/s and 0.05 kg/s. The cans distribution considered was staggered and in order arrangements. The maximum efficiency was obtained for staggered arrangement at 0.05 kg/s. Akpinar and Koçyiğit [23] conducted experimental work to study the flat plate SAH performance with various shaped obstacles attached to the absorber plate at different arrangements and angles. The results revealed that the SAH efficiency varied between 20% and 82%. Zomorrodian and Barati [24] presented an experimental study on solar air heaters with inclined perforated absorber plates with different porosities (perforation area to total area): 0.785, 1.786, and 3.314. From their results, it has been concluded that

the higher perforation design had maximum performance. Experiments have been analyzed on single- and double-pass SAHs with wire-mesh absorbers and perforated glass covers [25]. It was found that the double-pass solar collector achieved higher performance with 3-cm hole-to-hole spacing for a quarter-perforated cover at a mass flow rate of 0.032 kg/s. The thermal performance of three solar collectors with 3, 6 mm perforated single pass SAH and without perforated absorber were experimentally assessed by [26]. The SAH with a hole diameter of 3 mm had the highest efficiency with a temperature difference of 7 °C. Based on the review of previous studies, it can be concluded that there is a lack of information about studying the aspect of the factors' interaction in SAHs. The key parameters may interact with each other and cause different behaviors in contrast with their direct impact on SAHs' performance. Hence, the present study aims to conduct a parametric study about the interaction effect of the perforation ratio and Reynolds number on the perforated double pass solar air heater (PDPSAH) performance using the Design of Experiment (DOE) approach. Also, the present study focuses on determining the optimum parameters for maximum thermal performance of PDPSAH.

2.METHOD

The overall methodology of the present work can be explained in Fig. 1. The first step was to build up the test rig and decide on two influential parameters and three responses. The experimental work was conducted using the DOE approach to determine the empirical models and model-checking process. Finally, the optimum parameters were computed for maximum performance to decide the enhancement percentage that occurred using the developed SAH.

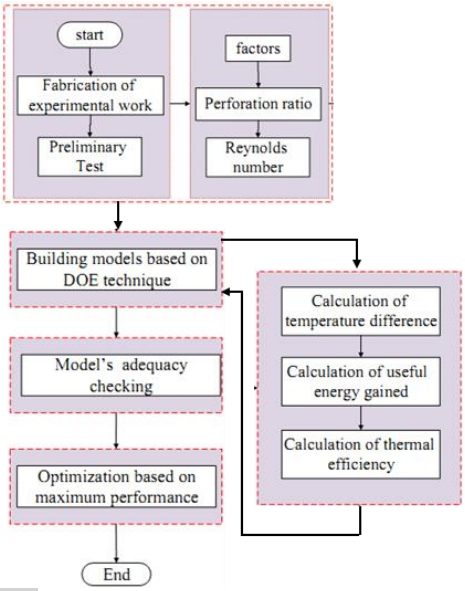

Fig. 1 Research Method of the Present Work.

2.1.Physical Model

The present setup was designed and manufactured from the available commercial materials. The main components of this setup comprise SAH, inlet and outlet sections, a blower, an air control valve, and a metal stand frame to fix these parts, as shown in Fig. 2.

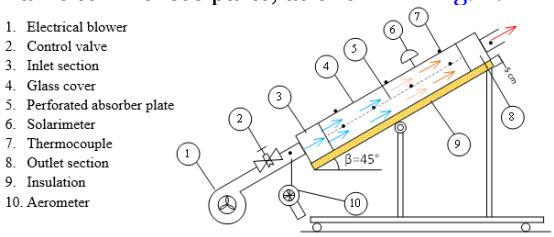

Fig. 2 Schematic of the Test Setup.

The SAH consists of an aluminum-made absorber plate, normal window glass as a cover, wooden walls, and foam as insulation 5 cm thick. The absorber plate's upper and lower faces were painted mat-black to increase its absorptivity to the solar radiation. To create two flow passes, the absorber plate was placed in the mid part of the SAH, and each channel's height became 5 cm, as illustrated in Fig. 3.

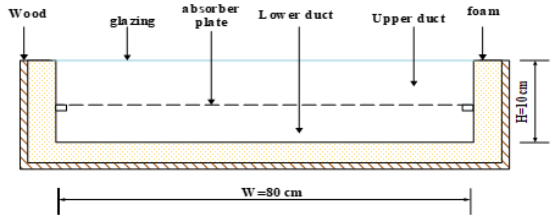

Fig. 3 Schematic Cross Section of SAH.

The air was forced through the SAH using the blower in which the flow stream was above and below the absorber plate at the same time. The perforated absorber plate allowed the air above and below the absorber to be exchanged across it, as demonstrated in Fig.4. Air mixing increased the turbulence intensity and enhanced the heat transferred from the hot perforated absorber plate to the air.

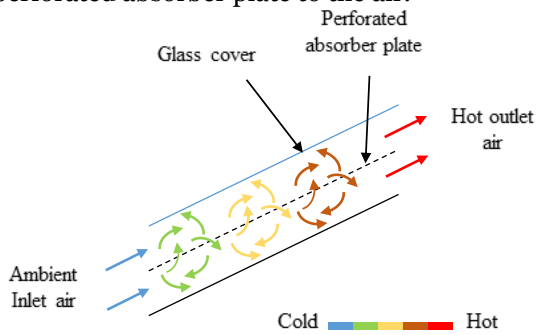

Fig. 4 Illustration of Perforation Effect on Flow in PDPSAH.

Three perforated absorber plates with staggered arrangements were considered. Each perforated absorber plate had one of three levels of perforation ratio (PR), i.e., the ratio of hole-to-hole pitch (s) to hole diameter (d). For comparison, another nonperforated (conventional) absorber plate was also tested. Figure 5 illustrates these three types of

configurations besides the conventional type. In addition, Table 1 summarizes the SAH specifications.

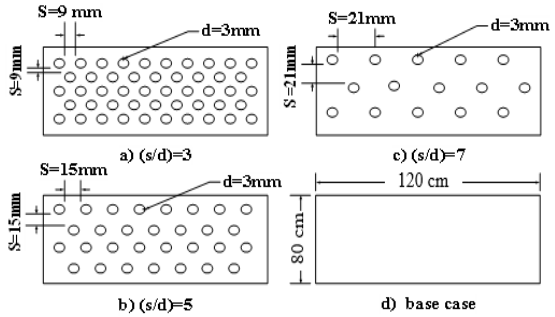

Fig. 5 Schematic of Four Types of Absorber Plates.

Table 1 Specifications of PDPSAH.

Components	Specifications
Absorber plate	Aluminum, 120 × 80 cm and 0.9 mm thickness
Perforation ratio	3, 5 and 7
Hole pitch	9, 15 and 21 mm
Hole diameter	3 mm for all perforated plates
glazing	Single glass cover, 0.4 cm thickness
Bottom and side Insulation	Foam, 5 cm thickness
Inlet section	Divergent passage, 60 cm length by 10 cm height
Outlet section	Convergent passage, 40 cm length by 10 cm height

2.2.Collector Thermal Efficiency

The instantaneous thermal efficiency of the system is defined as the ratio of the useful heat gain by the circulated air to the amount of incident solar radiation on the surface of the solar collector at any time [27].

$$\eta = \frac{Q_u}{IA_p} \quad (1)$$

The useful energy gained from the system is evaluated from:

$$Q_u = \dot{m} C_p \Delta T \quad (2)$$

Where the mass flow rate was calculated based on the continuity equation.

$$\dot{m} = \rho\, v\, A_i \quad (3)$$

The temperature difference is the difference between outlet and inlet air temperatures.

$$\Delta T = (T_{out} - T_{in}) \quad (4)$$

The overall (daily) efficiency (η_{day}) is calculated using the following formula:

$$\eta_{day} = \frac{\sum Q_u}{\sum I\, A_p} \quad (5)$$

While Reynolds number is defined as follows:

$$Re = \frac{\rho v D}{\mu} \quad (6)$$

The thermophysical properties of air, such as density (ρ_f) and viscosity (μ_f), are given as [28].

$$\rho_f = 3.9147 - 0.016082 T_{in} + 2.9013 \times 10^{-5} T_{in}^2 - 1.9407 \times 10^{-8} T_{in}^3 \quad (7)$$

$$\mu_f = (1.6157 + 0.06523 T_{in} - 3.0297 \times 10^{-5} T_{in}^2) \times 10^{-6} \quad (8)$$

The enhancement percentage in the thermal efficiency (Enh_η%) is defined as:

$$Enh_\eta\% = \frac{\eta_{PDPSAH} - \eta_{base\ case}}{\eta_{base\ case}} \times 100\ \% \quad (9)$$

While the enhancement in the useful heat gain (Enh_{Q_u}%) is expressed as:

$$Enh_{Q_u}\% = \frac{Q_{u PDPSAH} - Q_{u base\ case}}{Q_{u base\ case}} \times 100\ \% \quad (10)$$

The enhancement in the temperature difference ($Enh_{\Delta T}$%) is calculated from:

$$Enh_{\Delta T}\% = \frac{\Delta T_{PDPSAH} - \Delta T_{base\ case}}{\Delta T_{base\ case}} \times 100\ \% \quad (11)$$

Where the subscripts PDPSAH and base case pertained to the considered perforated SAH and nonperforated SAH, respectively.

2.3.Interaction of Factors Analysis

To clarify the interaction effect between factors, the difference in responses (ΔY) between the lower and higher levels of perforation ratio is given as:

$$\Delta Y_i = (Y_i)_{PR=3} - (Y_i)_{PR=7} \quad (12)$$

Where Y denotes the response (η, Qu, and ΔT), and the subscript (i) represents the value at any level of Reynolds number within the considered range. The interaction percentage can be defined as the increased percentage of the response difference (Y%) that can be mathematically written as:

$$Y\% = \left|\frac{\Delta Y_i - \Delta Y_1}{\Delta Y_1}\right| \times 100 \quad (13)$$

The subscript (1) corresponds to a low Reynolds number (Re = 10000).

2.4.Experimental Method

This section describes the instrumentation and the DOE approach of the present work experimental method. The PDPSAH oriented due south, as shown in Fig. 6, was experimentally tested under outdoor conditions in Tikrit City, Iraq. The geographical location is (34.35° N, 43.35° E) during (January, February, and March 2021). At minute interval measurements between (10:00 and 14:00), solar radiation, absorber temperatures at different locations, inlet and outlet temperatures, ambient air temperature, and glazing temperature were recorded. Type-k thermocouples connected to TC Series USB data acquisition (DAQ) data logger provided with eight channels measured temperature. The solar radiation was measured using the SL200 Kimo model solarimeter with a measuring range of (1-1300 W/m²). To ensure the maximum possible solar radiation incident on the SAH surface, it was tilted at 45° [2]. An air blower supplied air through the solar air heater. The blower was located at the solar collector inlet section and connected to a control valve to govern the amount of mass flow rate. A mini vane anemometer (UNI-T UT363), measuring range between (0-30 m/s) measured the inlet velocity. To construct a parametric experimental analysis, the DOE technique integrated with response surface methodology (RSM) was adopted in the present study. This method aims, firstly, to correlate the Reynolds number and perforation ratio with the PDPSAH performance and, secondly, to optimize the parameters under study based on the maximum

efficiency. This approach was conducted using Design-Expert 11 software. Two parameters, i.e., the Reynolds number and perforation ratio, were defined in the software, as illustrated in Table 2. The levels -1, 0, and 1 were the coded values of the considered parameters, while the real levels were 10000, 20000, and 30000 for the Reynolds number and 3, 5, and 7 for the perforation ratio, respectively.

Table 2 Experimental Factor Ranges Based on ±1 levels.

Parameter	Ranges and Levels			Unit
	-1	0	1	
Reynolds number (Re)	10000	20000	30000	-
Perforation ratio (PR)	3	5	7	-

The coded parameters can be derived as follows:

$$x_1 = \frac{Re - Re_0}{\Delta Re} \quad (14)$$

$$x_2 = \frac{PR - PR_0}{\Delta PR} \quad (15)$$

where x_1 and x_2 are the coded representations of the Reynolds number and perforation ratio, respectively. Re_0 and PR_0 are the middle-level values of the Reynolds number and perforation ratio, respectively. ΔRe and ΔPR are the intervals between the Reynolds number and perforation ratio values, respectively. The run sequence was generated by the software based on a face-centered composite design CCD [29], as listed in Table 3. Three responses, i.e., thermal efficiency, useful heat gain, and temperature difference, were investigated in the present study. The values of responses (η, Qu, and ΔT) corresponding to run number were obtained from experiments and entered in Design-Expert 11 software. The correlating model was suggested by the regression analysis based on the experimental results represented by the responses.

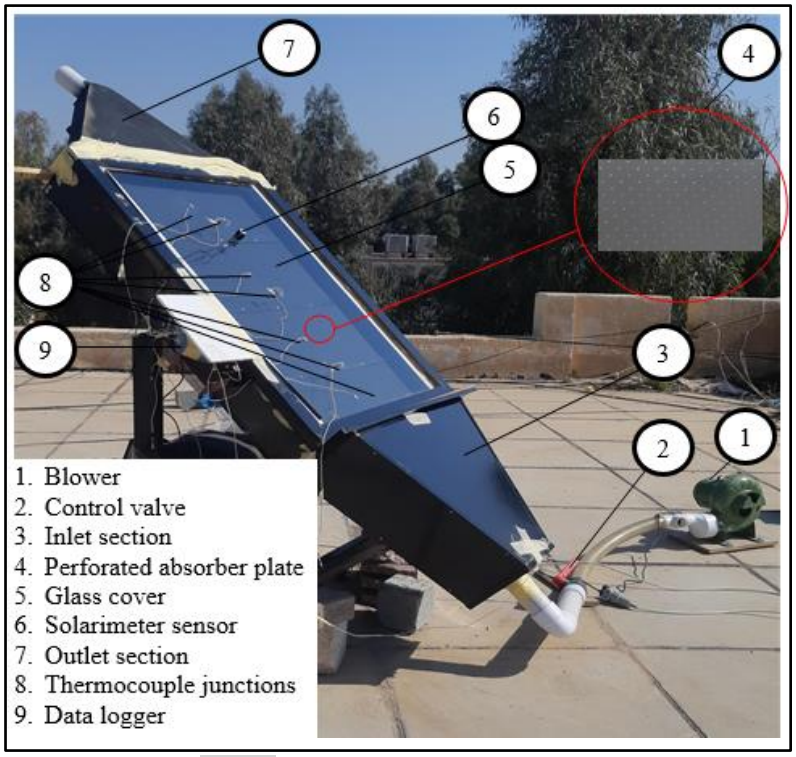

Fig. 6 Pictorial View of PDPSAH.

Table 3 The Process Factors and Responses.

Run	Factor 1 A: Re	Factor 2 B: PR	Response 1 η %	Response 2 *Qu* W	Response 3 ΔT °C
1	20000	5	49.51	478	23.5
2	20000	5	49.26	475	23.35
3	30000	7	51.35	503	16.94
4	30000	3	62.2	592.67	20.08
5	20000	3	51.79	495.84	24.31
6	20000	5	50.73	484	23.89
7	10000	7	44.26	427.86	41
8	10000	5	45.66	432.39	41.69
9	20000	5	49.9	476	23.47
10	20000	7	44.9	428	23.7
11	30000	5	58.25	578.64	19.29
12	10000	3	48.05	462.82	44.65

2.5.Uncertainty Analysis

The accuracy of experimental results is a significant aspect of developing reliable studies. Uncertainty analysis presents a powerful tool to study the measured data accuracy. The uncertainty estimation pertained to the dependent and independent parameters [30]. Considering a dependent parameter R as a function of the independent variables' numbers (X_1, X_2, X_3 …, X_r) as follows:

$$\mathbf{R = f(X_1, X_2, X_3 \dots, X_r)} \qquad \mathbf{(16)}$$

The independent variables uncertainties are ($U_{X_1}, U_{X_2}, U_{X_3}, \dots . U_{X_r}$), then the dependent variables uncertainty (U_R) can be calculated by:

$$\mathbf{U_R = \left[\left(\frac{\partial R}{\partial X_1} U_{X_1}\right)^2 + \left(\frac{\partial R}{\partial X_2} U_{X_2}\right)^2 + \left(\frac{\partial R}{\partial X_3} U_{X_3}\right)^2 + \dots + \left(\frac{\partial R}{\partial X_r} U_{X_r}\right)^2\right]^{\frac{1}{2}}} \qquad \mathbf{(17)}$$

The uncertainty and relative error values for the dependent and independent parameters are given in Table 4.

Table 4 Uncertainty and Relative Errors for Testing Parameters.

Parameter	Uncertainty	Relative Error %
Air temperature difference, ΔT	1.394 oC	5.89
Mass flow rate, $\dot{m}$	0.00273 kg/s	9.23
Reynolds number, Re	2874	9.58
Useful heat gain, Q_u	76.93 W	10.95
Thermal efficiency, η	0.0817%	12.04

3.RESULTS

3.1.Meteorological Data

The historical quarter-hourly solar irradiance variation was recorded and classified based on the Reynolds number value. For the Reynolds number of 10000, the measured solar irradiance and ambient temperature during the considered day hours are shown in Fig. 7. The measurements were performed on DOE testing days (2nd, 8th, and 14th of February 2021) when the Reynolds number of 10000 was adopted. The solar irradiance exhibited a nonsignificant difference between the days under study. Based on the DOE run order, the test days for Reynolds number 20000 were six days, as illustrated in Fig. 8, which shows the solar irradiance on these days. These test days were distributed over three months (January, February, and March). Despite that, the days have been selected for solar irradiance rates with nonsignificant differences. This methodology was suggested to reduce experimental errors due to non-uniform operation conditions. For Reynolds number 30000, the solar irradiance was measured through three days, as shown in Fig. 9. At around 11:00 AM, solar irradiance had an unnoticeable difference between its rates during test days. However, a slight difference was observed after midday time on the 24th of January. To observe the deviation of these metallurgical data from their average values, the standard deviation analysis was considered for all tests. The average value of solar irradiance for all test days was 995.19 W/m², while its standard deviation was 13.09 W/m². This result is evident in the uniform operation conditions adopted in the present work.

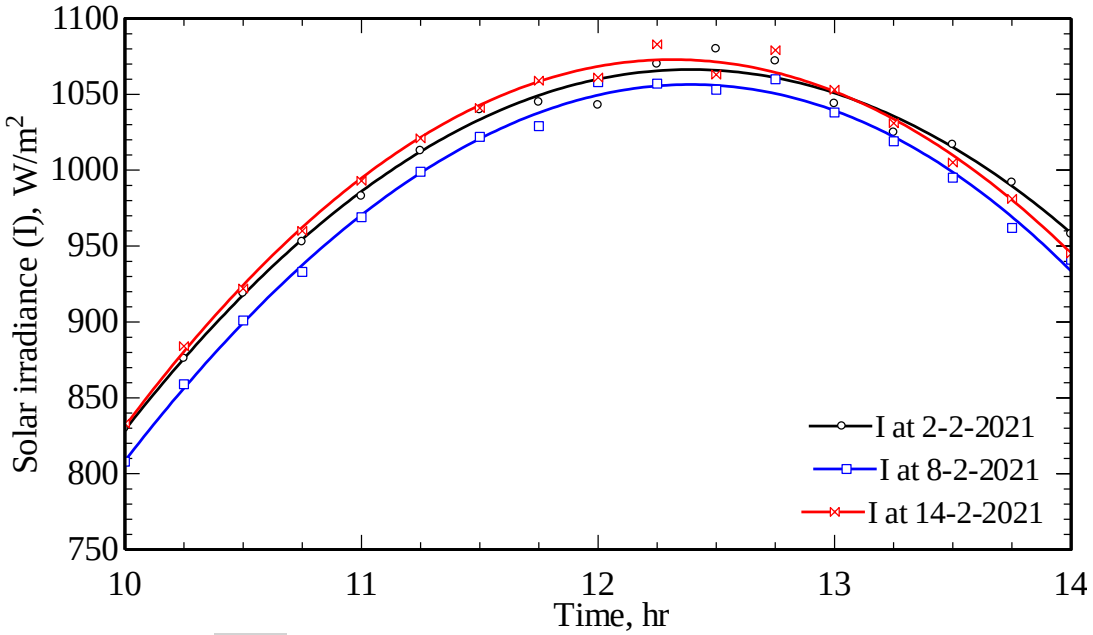

Fig. 7 Solar Irradiance at Different Days of Re = 10000.

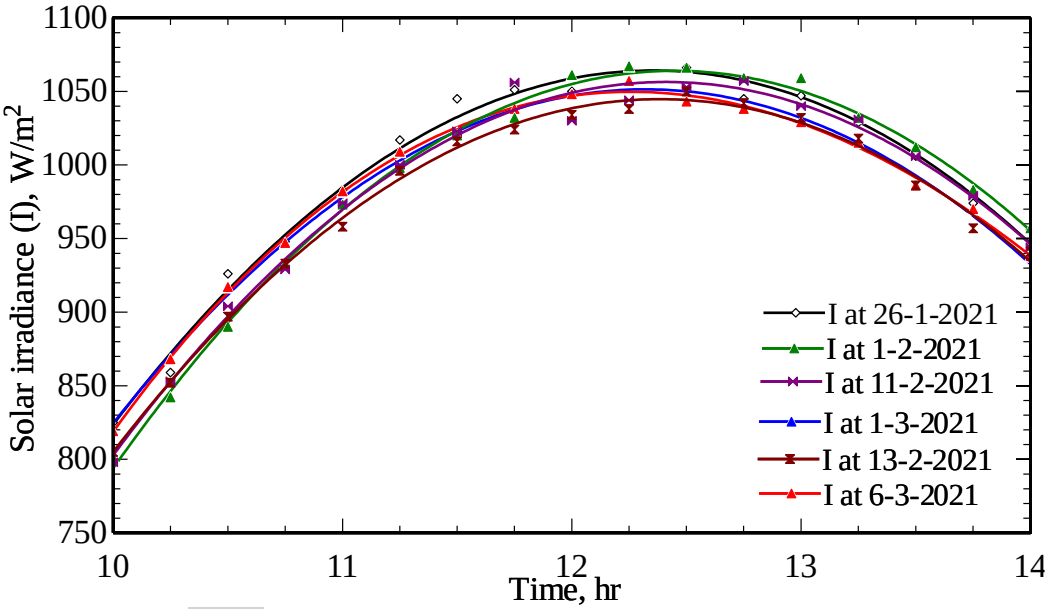

Fig. 8 Solar Irradiance at Different Days of Re = 20000.

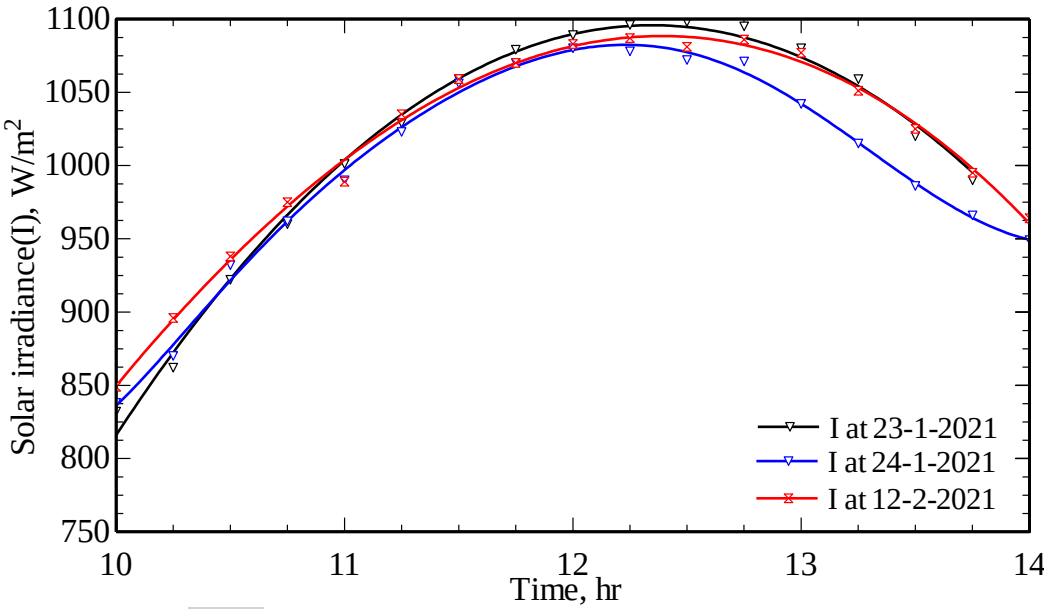

Fig. 9 Solar Irradiance at Different Days of Re = 30000.

3.2.Model Adequacy Examination

The suitable way to examine the model's adequacy is by testing the residuals, which are the differences between the actual and their corresponding estimation [31]. The normality assumption was checked by plotting the normal probability of residuals, as shown in Fig. 10 (a), (b), and (c), which illustrates the normal plot of residuals for the required responses. The plotted points fall near a straight line, indicating the error distribution normality. Also, for good models, the residuals should not be related to the predicted responses. As shown in Fig. 11 (a), (b), and (c), the externally studentized residuals are presented against the predicted response. The figure revealed no distinct patterns, indicating the residuals' independence on the predicted responses. The two lines above and below the zero-horizontal line ranged between (- 4.98253 and 4.98253) represent the limits of well distributed residual band. The residuals positioned out of this band are not noticed in this representation, and the experiments were scattered properly around the zero line of the residual. To check how far the correlating model could predict the required responses, the actual results computed from the experimental work are compared with those predicted ones. From Fig.12 (a), (b), and (c), the difference in residuals between the actual and predicted results is marginal and very small. These models give a very good impression of their adequacy and predictability for required responses (output) of PDPSAH with a high degree of accuracy.

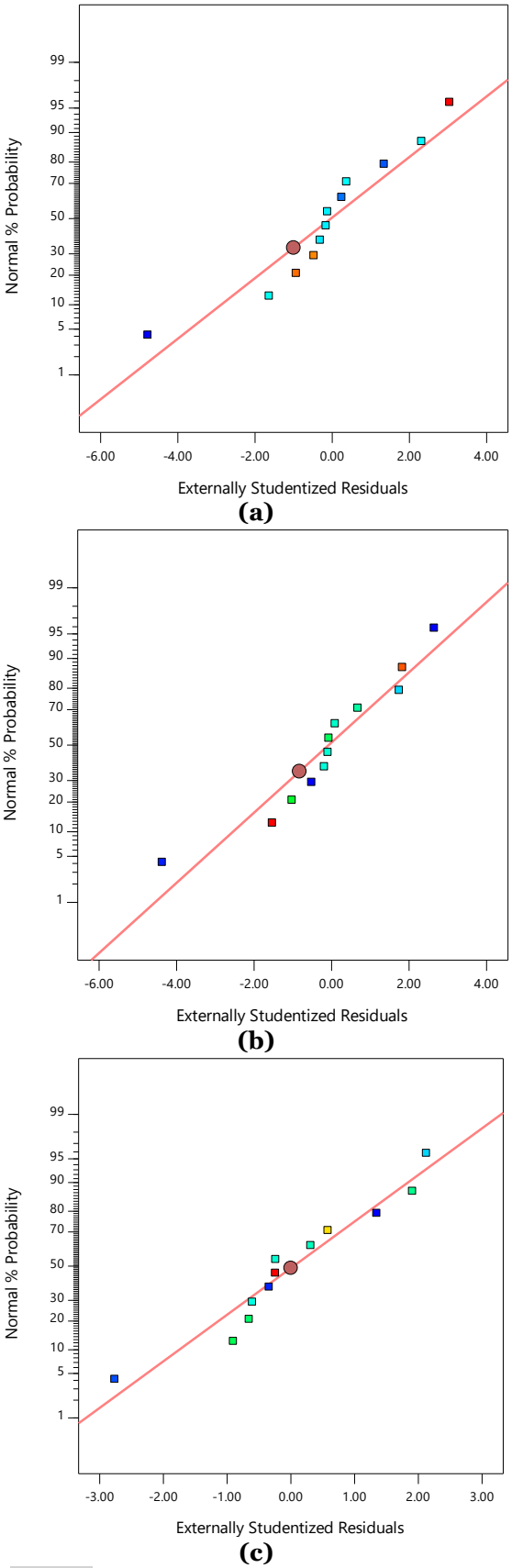

Fig. 10 Model Adequacy Checking by Testing Normal Probability of Residuals for (a) Temperature Difference, (b) Useful Heat Gain, and (c) Thermal Efficiency.

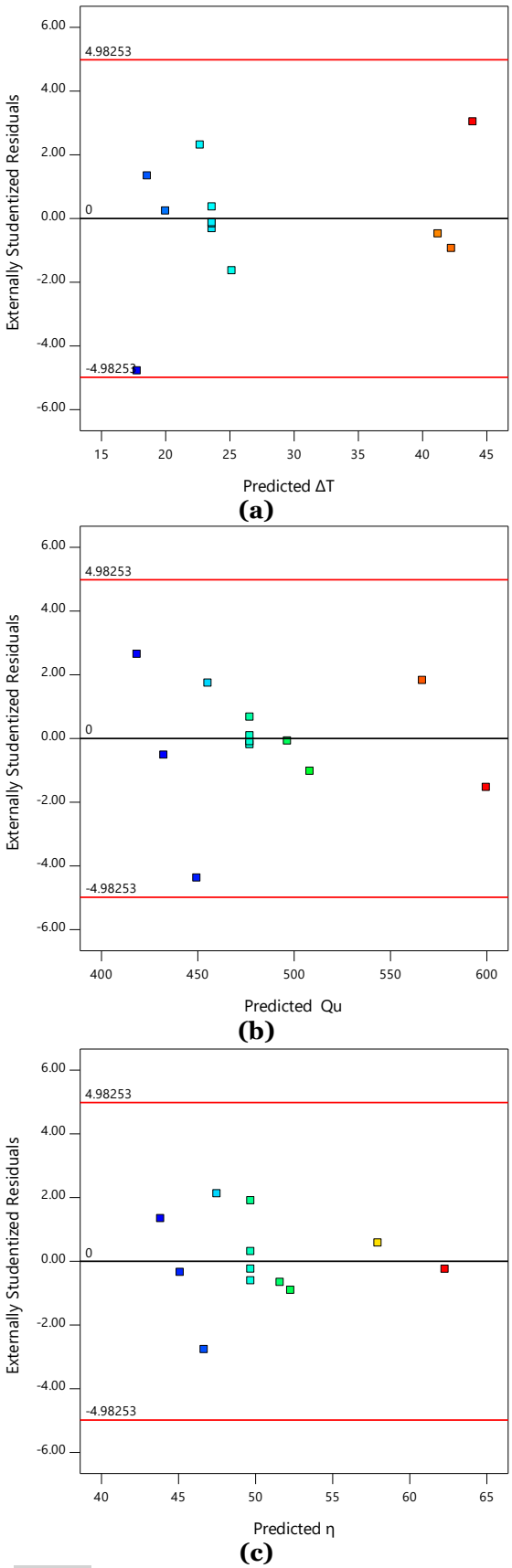

Fig. 11 Model Adequacy Checking by Testing the Independency of Residuals Predicted Response for (a) Temperature Difference, (b) Useful Heat Gain, and (c) Thermal Efficiency.

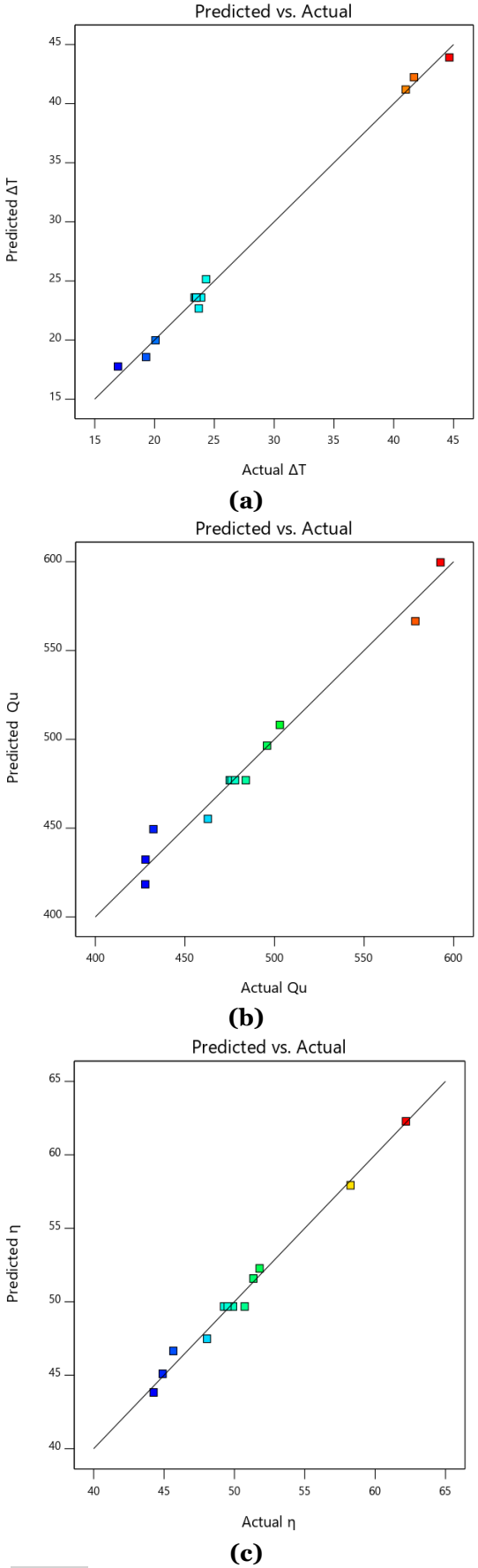

Fig. 12 Model Adequacy Checking by Testing Predicted and Actual Values Response for (a) Temperature Difference, (b) Useful Heat Gain, and (c) Thermal Efficiency.

3.3.Correlation Models

As mentioned earlier, central composite design (CCD) was used to develop models for the PDPSAH performance in terms of design parameters. For this aim, twelve runs integrated with four replicates (centered points) were involved to determine the correlations of responses in terms of actual (Re and PR) and coded factors (A and B). The sequential f-tests for (ΔT, Q_u, and η) proposed second-order polynomials where the additional terms were significant, and the models were not aliased. It is worthwhile to highlight the residuals (R-squared), which measure how well the model predicts the response value. In terms of actual forms, the final empirical correlations proposed by the software were as given below:

$$\eta = 42.77301 - 0.00004\,\mathrm{Re} + 2.46277\,\mathrm{PR} - 0.000088\,\mathrm{Re\,PR} + 2.61081\times10^{-8}\,Re^2 - 0.249436\,PR^2 \quad (18)$$

$$Q_u = 416.6667 - 0.003112\,\mathrm{Re} + 29.21208\,\mathrm{PR} - 0.000684\,\mathrm{Re\,PR} + 3.09642\times10^{-7}\,Re^2 - 3.15734\,PR^2 \quad (19)$$

$$\Delta T = 80.16284 - 0.003937\,\mathrm{Re} - 1.52684\,\mathrm{PR} + 6.34812\times10^{-6}\,\mathrm{Re\,PR} + 6.80232\times10^{-8}\,Re^2 + 0.078304\,PR^2 \quad (20)$$

while the coded form of these correlations is given as:

$$\eta = 49.68 + 5.64\,A - 3.59\,B - 1.76\,AB + 2.61\,A^2 - 0.9977B^2 \quad (21)$$

$$Q_u = 477.02 + 58.5\,A - 32.08\,B - 13.68\,AB + 30.96\,A^2 - 12.63\,B^2 \quad (22)$$

$$\Delta T = 23.60 - 11.84\,A - 1.23\,B + 0.127\,AB + 6.80\,A^2 + 0.3132\,B^2 \quad (23)$$

The reason behind presenting the correlations in coded form is to show the effects of variables on responses. The empirical relation for thermal efficiency of (R-squared = 0.9891) is given in Eq. (21). This correlation indicates that the weight effect of the Reynolds number, which is the most influential parameter, was about (5.64). While the effective weight of the perforation ratio was about (-3.59), which is greater than the half effect of the Reynolds number. Also, the coefficient that describes the interaction effective weights between the perforation ratio and Reynolds number, i.e., (AB), was about (-1.76). Similarly, the empirical correlation for useful heat gain in Eq. (22) with an R-squared value of 0.9762 exposed the studied parameters to approximately the same effective scenario. In contrast, the temperature difference correlation with (R-squared = 0.9960) is given in Eq. (23). Here, the effect of the perforation ratio is insignificant. In addition, the interaction effects of combined parameters vanished due to the very small effect weight of AB (coefficient = 0.127) compared to the A-coefficient of (-11.84). In summary, the above empirical models are valid

for the design parameters range and the conditions under which the present study was implemented. It can assess the PDPSAH performance to a high degree of accuracy. The final models show interesting results regarding the significance of factors under consideration. The empirical models revealed that the Reynolds number is the dominant factor in the performance of PDPSAH, followed by the perforation ratio.

3.4.Interaction of Factors

It is important to consider the interaction of input variables that avoid the conditions causing performance degradation in application areas. When the interaction effect is presented, the effect of one variable on the response is dependent on the level of the other factor. Based on each response, the present study considered the Reynolds number interaction with the perforation ratio. The interaction between both variables (PR and Re) was drawn by changing the perforation ratio at low and high levels and investigating the Reynolds number behavior. Since there are three responses under study in the present work, the interaction of factors was considered for each response. In this context, Fig. 13 depicts a clear interaction effect of the perforation ratio and Reynolds number on the thermal efficiency. At a low Reynolds number of around 10000, the increase in thermal efficiency was around 4% as the perforation ratio was decreased from 7 to 3. However, this effect gradually increased at higher Reynolds number values until it reached around 11% at the Reynolds number of 30000. Similarly, the interaction effect of the input parameters on the useful heat gain is illustrated in Fig. 14 and found to follow the same scenario of thermal efficiency. When the perforation ratio varied from 7 to 3, the useful heat gain increased approximately from 418 W to 455 W at a Reynolds number of 10000. On the other hand, at a Reynolds number of 30000, the useful heat gain increased approximately from 508 W to 599 W when the perforation ratio varied from 7 to 3. In contrast, the interaction effect on temperature difference across the SAH is depicted in Fig. 15. The temperature difference is inversely proportional to the Reynolds number, while the curves are parallel. In other words, when the perforation ratio decreased from 7 to 3, the interaction effect was insignificant at all Reynolds number values. To clarify the interaction effect between factors, the interaction percentage has been plotted for the three responses under study, as shown in Fig. 16. Obviously, the interaction started from zero point at Reynolds number of 10000 and approached around 193% for efficiency and 148% for useful heat gain, while it did not exceed 18% for temperature difference at Reynolds number of 30000.

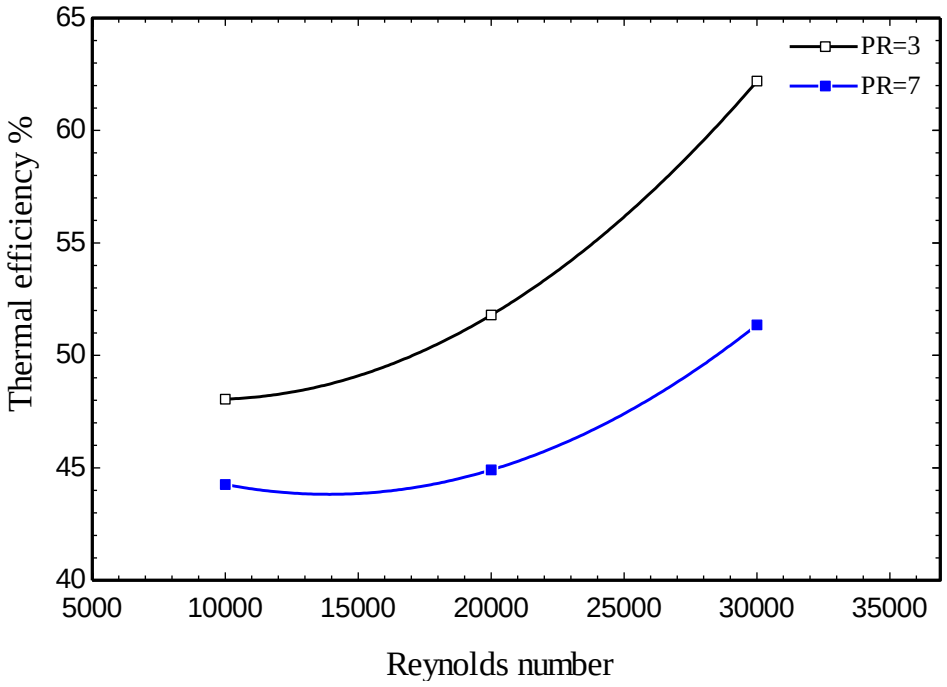

Fig. 13 Interaction of Reynolds Number and Perforation Ratio and their Effect on Thermal Efficiency.

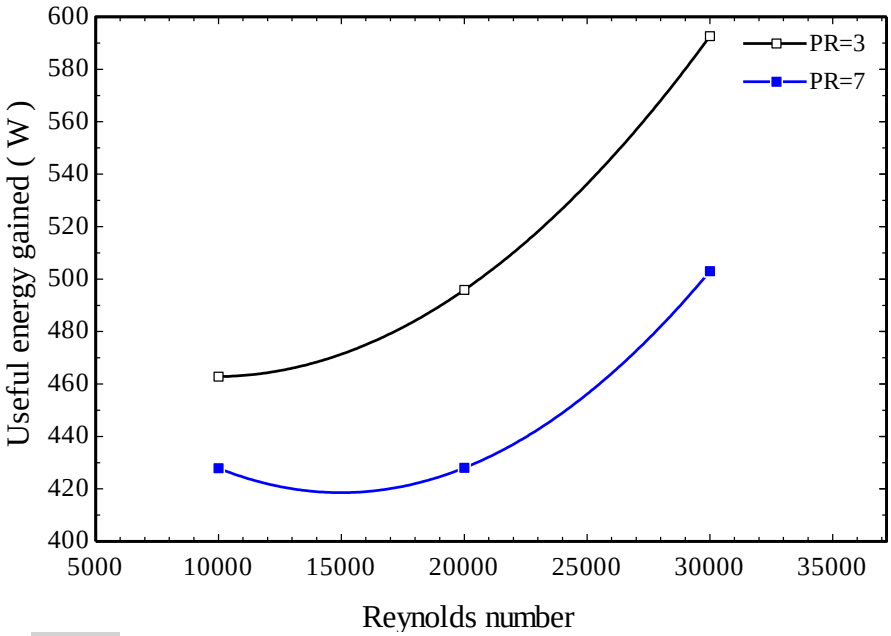

Fig. 14 Interaction of Reynolds Number and Perforation Ratio and Their Effect on Useful Heat Gain.

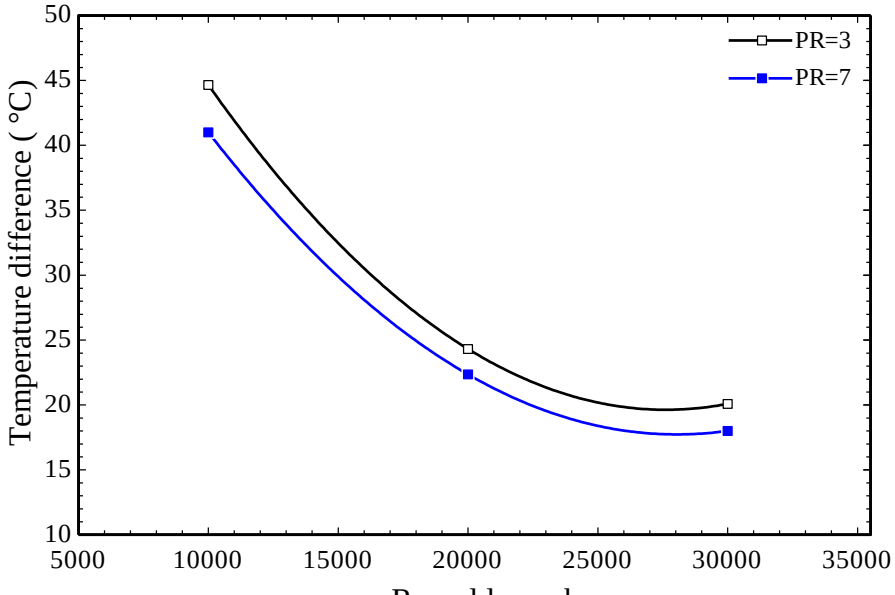

Fig. 15 Interaction of Reynolds Number and Perforation Ratio and Their Effect on Temperature Difference.

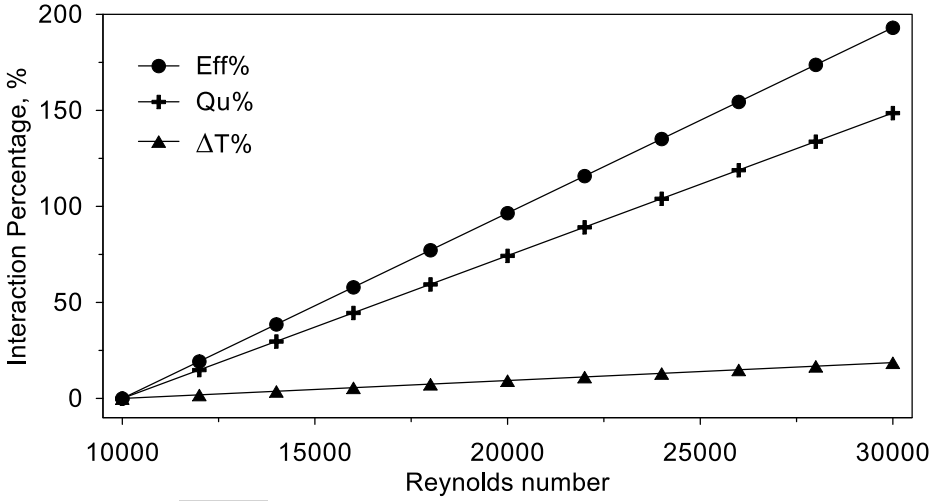

Fig. 16 The Percentage of Interaction of Factors.

3.5.Models Optimization

3.5.1.Optimization Criteria

One of the main objectives of this work is to find the optimum conditions (process parameters) to maximize the PDPSAH performance. The optimization process was performed using Design Expert software. The optimization criterion was based on setting the responses (ΔT, Q_u, and η) as maximum as possible. Meanwhile, the influential factors were set in range. Each process factor's goal and the responses were identified as an optimization criterion, as given in Table 5. In summary, the maximum responses are targeted when the factors are in range.

Table 5 Range of Input Parameters and Responses for Optimization.

Parameter	Goal	Lower Limit	Upper Limit
Re	In range	10000	30000
PR	In range	3	7
η_{th}	Maximize	44.26	62.2
Q_u	Maximize	427.86	599.6
ΔT	Maximize	16.94	44.65

3.5.2.Optimum Conditions and Enhancement Percentage

The optimization analysis was performed, and the optimal operating conditions obtained based on the input parameter's criteria are given in Table 6. The Reynolds number was 30000 as an input factor, while the perforation ratio was 3 for the PDPSAH maximum performance. The maximum responses recorded for thermal efficiency was 62.2%, useful heat gain was 599.6 W, and temperature difference was 19.98 °C. To determine the enhancement in the PDPSAH performance due to perforation, a base case test was conducted using a nonperforated DPSAH at the same operation conditions. The results revealed that the enhancement percentages in the performance of PDPSAH compared to the base case were 12.36%, 11.11%, and 9.7% for η, Q_u, and ΔT, respectively.

Table 6 Optimum Values of Input Parameters, Responses, and Percentage Enhancement.

Parameter	Optimum Value	Base Case	Enhancement %
Re	30000	30000	-
PR	3	-	-
η_{th}	62.2	55.35	12.36
Q_u	599.6	540.9	11.11
ΔT	19.98	18.21	9.7

3.5.3.Optimum Response Surface Representation

To provide a clear picture of the optimum responses' behavior due to parameter variations, a 3D surface representation and constant response lines (contour lines) are presented. Figure 17 shows that the effect of the Reynolds number and perforation ratio on the thermal efficiency behaves as a concave in the Reynolds number's direction and as a convex in the perforation ratio's direction. The highest point of this surface represents the maximum efficiency of 62.2% at Reynolds number of 30000 and perforation ratio of 3. The convex shape indicates the possibility of the existence of the peak point in the case of reducing the perforation ratio to levels less than 3. In other words, increasing the hole numbers more than the limit this study considered may reduce the PDPSAH thermal efficiency. The constant response lines reflect the response surface behavior in more detail. A difference in behavior can be observed for the constant response lines between the regions near the point (Re = 30000 and PR = 3) and point (Re = 10000 and PR = 7). This behavior indicates the existence of interaction between factors, as discussed previously.

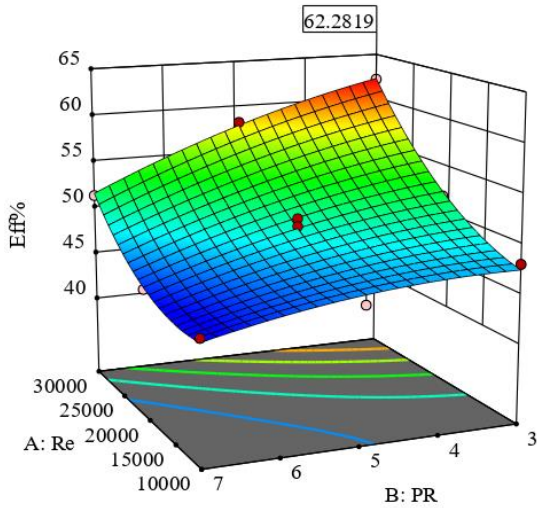

Fig. 17 Thermal Efficiency Contour and 3D Surface Shape Formed by the Effect of Perforation Ratio and Reynolds Number at Optimum Operating Conditions.

Similarly, the response surface of the useful heat gain revealed the same scenario of a curvature shape behavior of the thermal efficiency, as exhibited in Fig. 18. The response surface of the useful heat gain shows the convex trend in perforation ratio direction but a concave shape in Reynolds number direction. Within the current ranges of the parameters under consideration, the useful heat gain surface had a higher point of around 599.6 W at Reynolds number of 30000 and perforation ratio of 3. However, the convex shape in the direction of the perforation ratio axis indicates a peak point if the perforation ratio range has extended to less than 3. The constant response lines of useful heat gain show a similar variety as the efficiency with the Reynolds number and perforation ratio. The interaction of factors observed in the previous section supports the same result of the contour line trend.

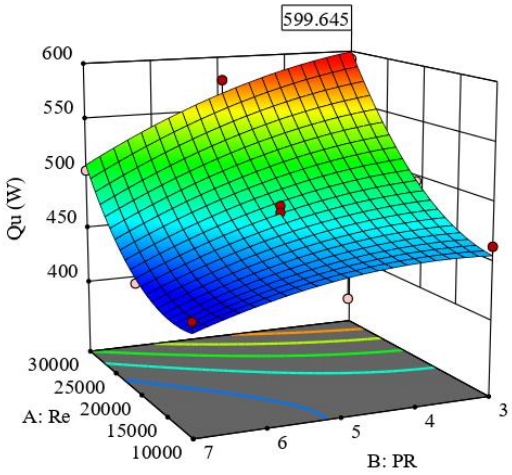

Fig. 18 Useful Energy Gain Contour and 3D Surface Shape Formed by the Effect of Perforation Ratio and Reynolds Number at Optimum Operating Conditions.

The response surface pertained to temperature difference is depicted in Fig. 19. In contrast with efficiency and useful heat gain, it can be observed that the response surface of the temperature difference changes linearly in the perforation ratio axis direction, while it has a curvature shape when the Reynolds number changes. The constant response lines of the temperature difference also illustrate this behavior. Also, the nonsignificant interaction of factors discussed reflects this result for the temperature difference.

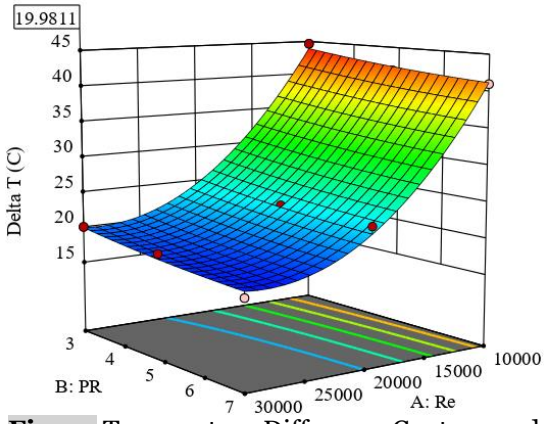

Fig. 19 Temperature Difference Contour and 3D Surface Shape Formed by the Effect of Perforation Ratio and Reynolds Number at Optimum Operating Conditions.

In conclusion, increasing the hole number in the absorber plate or using a lower perforation ratio is the best choice for obtaining maximum performance. This result is because exchanging larger air mass through holes of the absorber plate captures more heat from the upper and lower surfaces of the absorber due to an increase in turbulence level. Consequently, higher thermal efficiency values, energy gain, and temperature difference were attained. This result agrees well with the results concluded in previous work [24] and is proven by another study [26].

4.CONCLUSIONS

The present work introduces a double-pass solar air heater using a perforated absorber plate. Experimental work has been conducted to assess the perforated solar collector's performance. The following conclusions can be extracted from this work: Essentially, it is known that the decrease in surface area reduces the heat transfer rates and the SAH thermal performance. The less perforation ratio means cutting out more material from the absorber plate. In other words, minimizing the perforation ratio lessens the surface area occupied by the absorber plate material within the gross SAH area. However, maximum thermal efficiency is obtained as the perforation ratio tends to a minimum value within the range considered in the present work. This enhancement in performance is attributed to the impact of flow disturbance induced by momentum exchange through the holes between the PDPSAH's upper pass and the lower pass. The reduction in perforation ratio augments the flow turbulence, affecting the area reduction effect dominance at lower perforation ratio values, which interprets why the efficiency of base case (nonperforated SAH) had a value of (55.35%) between the minimum and maximum values, i.e., 44.26% and 62.2% of the PDPSAH efficiency correspond to higher and lower perforation ratio values (7 and 3), respectively. The DOE analysis is a perfect tool to study the interesting effects between factors by considering the interaction of factors. Based on the interaction between the Reynolds number and perforation ratio, the enhancement for the present design compared to the base case is observed at high Reynolds number values while disappearing at low Reynolds number values. In other words, the efficiency value of nonperforated SAH does not fall between the perforated SAH minimum and maximum values at low Reynolds number values under consideration, while it does at higher Reynolds number values. Thus, no enhancement is recorded in terms of thermal efficiency due to the insignificant effect of turbulence at low Reynolds number values. The considered ranges of the perforation ratio and Reynolds number are worthy of adopting for determining the starting point of enhancement. However, higher efficiency may be obtained at the perforation ratio and Reynolds number values out of the studied ranges. In conclusion, the PDPSAH optimum performance requires wider ranges of the perforation ratio and Reynolds number to be investigated.

ACKNOWLEDGEMENT

The authors are grateful to Tikrit University, College of Engineering, for their valuable support in providing experimental measuring instrumentation to accomplish this work.

NOMENCLATURE

A_p	Collector surface area, m^2
A_i	Entrance port area, m^2
C_p	Specific heat of air, J/kg. k
D	Diameter of entrance port, m
I	Solar irradiance, W/m^2
$\dot{m}$	Mass flow rate, kg/s
Q_u	Useful energy gain, W
Re	Reynolds number
T_{out}	Outlet temperature, ℃
T_{in}	Inlet temperature, ℃
v	Velocity, m/s
Greek symbols	
η	Thermal efficiency
ρ	Density, kg/m^3
μ	Dynamic viscosity, kg/m. s
ΔT	Temperature difference, ℃
Subscript	
PDPSAH	Perforated double pass solar air heater
Base case	Base case SAH (nonperforated absorber)

REFERENCES

[1] González SM, Larsen SF, Hernández A, Lesino G. **Thermal Evaluation and Modeling of a Double-Pass Solar Collector for Air Heating**. *Energy Procedia* 2014; **57**:2275-2284.

[2] Alam T, Kim M-H. **Performance Improvement of Double-Pass Solar Air Heater–a State of Art of Review**. *Renewable and Sustainable Energy Reviews* 2017; **79**:779-793.

[3] Kabeel A, Hamed MH, Omara Z, Kandeal A. **Influence of Fin Height on the Performance of a Glazed and Bladed Entrance Single-Pass Solar Air Heater**. *Solar Energy* 2018; **162**:410-419.

[4] Abdulmalek SH, Al-Kayiem HH, Assadi MK, Gitan AA. **Development of Multi Chamber Technique to Improve the Uniformity in Drying Application**. *6th International Conference on Production, Energy and Reliability 2018: World Engineering Science & Technology Congress (ESTCON)* 2018; Kuala Lumpur, Malaysia: p. 020007.

[5] Murali G, Nandan BS, Reddy NSK, Teja D, Kumar NK. **Experimental Study on Double Pass Solar Air Heater with Fins at Lower and Upper Channel**. *Materials Today: Proceedings* 2020; **21**:578-583.

[6] Gupta M, Kaushik S. **Exergetic Performance Evaluation and Parametric Studies of Solar Air Heater**. *Energy* 2008; **33**(11):1691-1702.

[7] Mohammadi K, Sabzpooshani M. **Comprehensive Performance Evaluation and Parametric Studies of Single Pass Solar Air Heater with Fins and Baffles Attached over the Absorber Plate**. *Energy* 2013; **57**:741-750.

[8] Yıldırım C, Solmuş İ. **A Parametric Study on a Humidification–Dehumidification (Hdh) Desalination Unit Powered by Solar Air and Water Heaters**. *Energy Conversion and Management* 2014; **86**:568-575.

[9] Verma P, Varshney L. **Parametric Investigation on Thermo-Hydraulic Performance of Wire Screen Matrix Packed Solar Air Heater**. *Sustainable Energy Technologies and Assessments* 2015; **10**:40-52.

[10] Kumar A, Layek A. **Energetic and Exergetic Based Performance Evaluation of Solar Air Heater Having Winglet Type Roughness on Absorber Surface**. *Solar Energy Materials and Solar Cells* 2021; **230**:111147.

[11] Parsa H, Saffar-Avval M, Hajmohammadi M. **3D Simulation and Parametric Optimization of a Solar Air Heater with a Novel Staggered Cuboid Baffles**. *International Journal of Mechanical Sciences* 2021; **205**:106607.

[12] Acır A, Canlı ME, Ata İ, Çakıroğlu R. **Parametric Optimization of Energy and Exergy Analyses of a Novel Solar Air Heater with Grey Relational Analysis**. *Applied Thermal Engineering* 2017; **122**:330-338.

[13] Kumar R, Kumar A, Goel V. **A Parametric Analysis of Rectangular Rib Roughened Triangular Duct Solar Air Heater Using Computational Fluid Dynamics**. *Solar Energy* 2017; **157**:1095-1107.

[14] Goel V, Kumar R, Bhattacharyya S, Tyagi V, Abusorrah AM. **A Comprehensive Parametric Investigation of Hemispherical Cavities on Thermal Performance and Flow-Dynamics in the Triangular-Duct Solar-Assisted Air-Heater**. *Renewable Energy* 2021; **173**:896-912.

[15] Dezan DJ, Rocha AD, Ferreira WG. **Parametric Sensitivity Analysis and Optimisation of a Solar Air Heater with Multiple Rows of Longitudinal Vortex Generators**. *Applied Energy* 2020; **263**:114556.

[16] El-Khawajah M, Aldabbagh L, Egelioglu F. **The Effect of Using Transverse Fins on a Double Pass Flow Solar Air Heater Using Wire Mesh as an Absorber**. *Solar Energy* 2011; **85**(7) :1479-1487.

[17] Mahmood A, Aldabbagh L, Egelioglu F. **Investigation of Single and Double Pass Solar Air Heater with Transverse Fins and a Package Wire Mesh Layer**. *Energy Conversion and Management* 2015; **89**:599-607.

[18] Sharma A, Varun, Kumar P, Bharadwaj G. **Heat Transfer and Friction**

Characteristics of Double Pass Solar Air Heater Having V-Shaped Roughness on the Absorber Plate. *Journal of Renewable and Sustainable Energy* 2013; **5**(2):023109.

[19] Tated MK, Singh DP, Dogra S. **Heat Transfer and Friction Factor Characteristics of Double Pass Solar Air Heater Using W-Shaped Artificial Roughness Ribs**. *IOSR Journal Of Mechanical And Civil Engineering (IOSR-JMCE)* 2015; 2278-1684.

[20] Mohammed MF, Eleiwi MA, Kamil KT. **Experimental Investigation of Thermal Performance of Improvement a Solar Air Heater with Metallic Fiber**. *Energy Sources, Part A: Recovery, Utilization, and Environmental Effects* 2021; **43**(18): 2319-2338.

[21] Eleiwi MA, Shallal HS. **Thermal Performance of Solar Air Heater Integrated with Air–Water Heat Exchanger Assigned for Ambient Conditions in Iraq**. *International Journal of Ambient Energy* 2022; **43**(1): 2153-2164.

[22] Ozgen F, Esen M, Esen H. **Experimental Investigation of Thermal Performance of a Double-Flow Solar Air Heater Having Aluminium Cans**. *Renewable Energy* 2009; **34**(11):2391-2398.

[23] Akpinar EK, Koçyiğit F. **Energy and Exergy Analysis of a New Flat-Plate Solar Air Heater Having Different Obstacles on Absorber Plates**. *Applied Energy* 2010; **87**(11):3438-3450.

[24] Zomorrodian A, Barati M. **Efficient Solar Air Heater with Perforated Absorber for Crop Drying**. 2010.

[25] Nowzari R, Mirzaei N, Aldabbagh L. **Finding the Best Configuration for a Solar Air Heater by Design and Analysis of Experiment**. *Energy Conversion and Management* 2015; **100**: 131-137.

[26] Farhan AA, Sahi HA. **Energy Analysis of Solar Collector with Perforated Absorber Plate**. *Journal of Engineering* 2017; **23**(9):89-102.

[27] Chabane F, Moummi N, Benramache S. **Experimental Study of Heat Transfer and Thermal Performance with Longitudinal Fins of Solar Air Heater**. *Journal of Advanced Research* 2014; **5**(2):183-192.

[28] Mortazavi A, Ameri M. **Conventional and Advanced Exergy Analysis of Solar Flat Plate Air Collectors**. *Energy* 2018; **142**:277-288.

[29] Qader BS, Supeni E, Ariffin M, Talib AA. **RSM Approach for Modeling and Optimization of Designing Parameters for Inclined Fins of Solar Air Heater**. *Renewable Energy* 2019; **136**:48-68.

[30] Holman JP. **Analysis of Experimental Data**. In: Holman JP. Experimental Methods for Engineers. New York, USA: McGraw-Hill; 2001.

[31] Gitan A. **Flow Characteristics and Heat Transfer Enhancement at Interference Zone of Twin Pulsating Circular Jets**. National University of Malaysia Bangi, Selangor, Malaysia; 2015.